Supporting Information

Extraordinary Magnetic Field Effects Mediated by Spin-Pair Interaction and Electron Mobility in Thermally Activated Delayed Fluorescence-Based OLEDs with Quantum Well Structure

Ruiheng Pan,[a] Xiantong Tang,[a] Yeqian Hu,[a] Hongqiang Zhu,[a] Jinqiu Deng,[a] and Zuhong Xiong*[a]

[a]*School of Physical Science and Technology, MOE Key Laboratory on Luminescence and Real-Time Analysis, Southwest University, Chongqing 400715, People's Republic of China*

**E-mail: zhxiong@swu.edu.cn*

1. Optical property of CBP and 4CzTPN-Ph

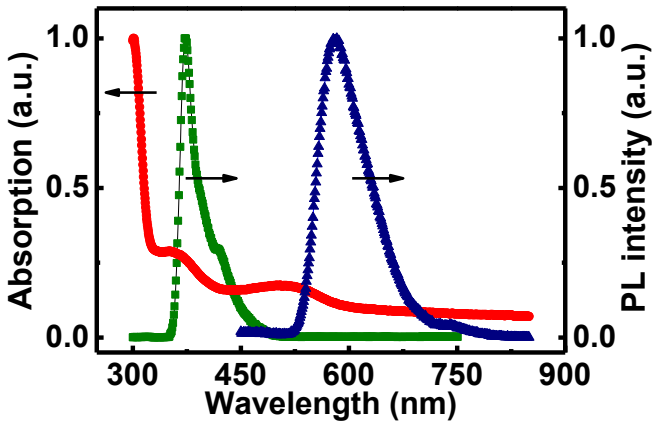

Fig. S1 The normalized optical absorption spectrum of 4CzTPN-Ph, the photoluminescence spectra of CBP and 4CzTPN-Ph.

As shown in Fig. S1, the emission spectrum of CBP at 370 nm overlaps significantly with the absorption spectrum of 4CzTPN-Ph ranging from 360 nm to 440 nm. This indicated that the energy transfer processes between PBL and PWL would occur through the single step long-range Förster-type transfer,[1-3] leading to the increased quantities of 4CzTPN-Ph ^{1}CT excitons.

2. The structure and energy level of Dev. 2

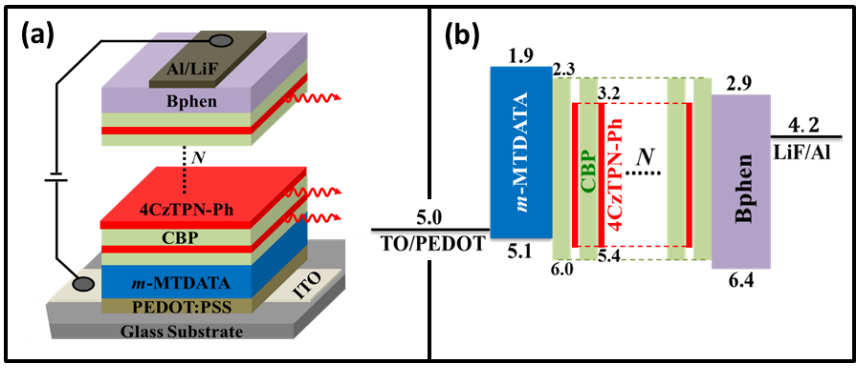

Fig. S2 The structure (a) and energy level (b) of Dev. 2.

The structure and energy level of Dev. 2 are shown in Fig. S2, respectively. The detailed fabrication and measurement processes for the Dev. 2 have been given in the Experimental

section. As can be seen, the HOMO gap (0.4 eV) between CBP and Bphen is relatively small, leading to the few accumulations of holes in CBP layer near the CBP/Bphen interface. Consequently, the TQA dissociation channel is largely suppressed in Dev. 2 as compared to Dev. 1 due to its high HOMO gap (1.0 eV) between CBP and BCP.

3. The EL spectra and I-V curves of Dev. 1 and Dev. 2

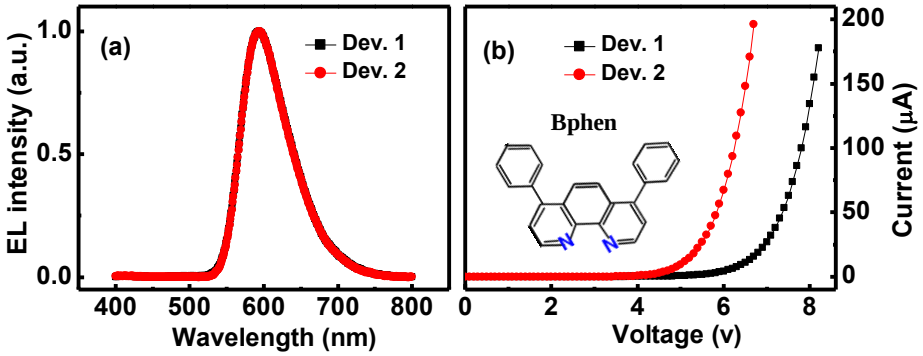

Fig. S3. (a) Normalized EL spectra of Dev. 1 and Dev. 2; (b) Current-voltage curves of Dev. 1 and Dev. 2, the inset of panel (b) shows the molecular structure of Bphen.

Fig. S3 shows the EL spectra and *I-V* curves for Dev. 1 and Dev. 2. It is observed that their EL peaks are coincided with each other (Fig. S3a), which both are peaked at ~590 nm. This indicated that there is only light-emission from 4CzTPN-Ph in Dev. 1 and Dev. 2. Moreover, it means that the energy transfer types occurred within Dev. 1 and Dev. 2 are consistent with each other. Bphen is a kind of typical electron transporting material due to its high electron mobility.[4-6] Obviously, based on the fact that other organic functional layers remain unchanged except for the electron transporting material, the turn-on voltage of Dev. 2 is lower than that of Dev. 1 since the electron mobility of Bphen is larger than that of BCP,[4] which is evidenced by the Fig. S3b.

4. Impaction of electron transporting layer on MFE curves from QW-TADF-OLEDs with N = 7

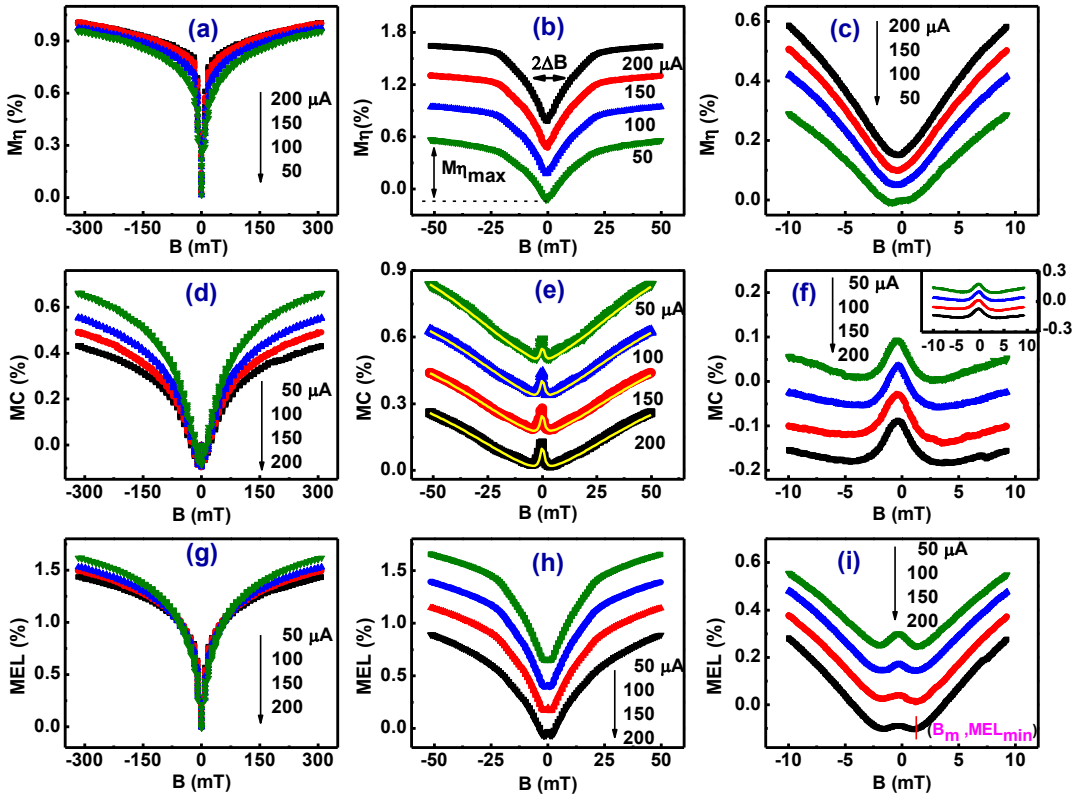

Fig. S4 The current-dependent Mη, MC, and MEL curve of Dev. 2. Panels (b), (c), (e), (f), (h), and (i) are shifted vertically for clarity. Among them, $M\eta_{max}$ is saturation Mη value at large B. ΔB is HWHM, as defined in (b). (e) The measured MC curves (hollow symbol) and their corresponding fitted lines (yellow solid line). In order to clearly compare and analyze the fine structures in the MC and MEL traces within $|B| < 5$ mT, we make big vertical shift for the MC traces in (f) and replot them in the inset of (f) by the almost same amplitude value (0.6%) of the whole y-coordinate as the MEL traces have in (i). Upon decreasing B the MEL curve within $|B| < 10$ mT reached a minimum value (MEL_{min}) at $B = B_m$, as defined in (i).

To further assess the effect of the electron transporting layer on the MFEs of QW-TADF-OLEDs (N=7), we designed and fabricated an OLED with the structure of ITO/PEDOT:PSS/*m*-MTDATA(40 nm)/[CBP(3.75 nm)/4CzTPN-Ph(0.5 nm)]$_{N=7}$/CBP (3.75 nm)/Bphen(50 nm)/LiF(1 nm)/Al(120 nm) (Dev. 2), whose device structure and energy level are displayed in Fig. S2. The current-dependent MFE curves of Dev. 2 at various magnetic

field ranges are shown in Fig. S4. It can be clearly seen that both the Mη (Figs. S4a, 4b, and 4c) and MEL (Figs. S4g, 4h, and 4i) curves of Dev. 2 exhibited similar trends to those observed in Mη and MEL curves of Dev. 1 (Figs. 2a, 2b, and 2c and Figs. 2g, 2h, and 2i). Moreover, they respectively displayed V-type and more obvious W-like line-shapes as compared to Dev. 1 within $|B|< 10$ mT (Figs. S4c and 4i). Therefore, according to the analysis in section 3.2, the RISC of 4CzTPN-Ph CT excitons in each PWL and ISC of CBP polaron pairs in each PBL collectively determined the line-shape of Mη curves in Figs. S4a, 4b, and 4c. Clearly, the ISC process is dominant because each CBP layer is thicker than each 4CzTPN-Ph layer, leading to the positive V-type line-shape in Fig. S4c. In addition, we speculated that more obvious W-like line-shapes observed in Fig. S4i should be attributed to the combined influences of MC and Mη curves and the relevant discussion is as follows.

Obviously, Fig. S4d shows that MC behaviors of Dev. 2 are similar to that of Dev. 1 at $|B| < 300$ mT (Fig. 2d), further implying that four spin-pair interactions (primarily including ISC of CBP polaron pairs, RISC of 4CzTPN-Ph CT excitons, and TQA dissociation and scattering processes) indeed exist in these two kinds of QW-TADF-OLEDs. However, contrary to the fine measurement in Dev. 1 (Fig. 2e), it is noteworthy that the non-platform structure can be observed in the Dev. 2 at $|B|<50$ mT (Fig. S4e). More specifically, the MC traces within $|B| < 50$ mT exhibit a W-like line-shape consisting of two components: (i) a rapid drop within $|B| < 3$ mT; (ii) a gradual enhancement within $20 < |B| < 50$ mT. According to the explanation in section 3.3, there is no doubt that the decreased part of MC curves within $|B| < 3$ mT is originated from the superposition of ISC (CBP polaron pairs) and RISC (4CzTPN-Ph CT excitons). By analyzing the structure and energy level diagram of Dev. 2

(Fig. S2), it is confirmed that the small LUMO gap (0.6 eV) between CBP and Bphen contribute to the increased injection of electrons, causing that electrons become majority carriers in the device. In addition, since the electron mobility of Bphen is larger than that of BCP, the transmission of electrons from Bphen to CBP in Dev. 2 is easier than that from BCP to CBP in Dev. 1, leading to the lower turn-on voltage of Dev. 2 than that of Dev. 1 (Fig. S3b). Moreover, the majority electrons are easily scattered by T_1 excitons of CBP and ^{3}CT excitons of 4CzTPN-Ph, and these TQA scattering processes could be mediated by applied magnetic fields,[7] producing the disappearance of platform in the MC curves of Dev. 2.

Similarly, eqn (2) was also used to fit the MC experimental data in Fig. S4e to further prove the correctness of above discussion, and the fitted curves are shown by the yellow solid lines in Fig. S4e. It can be clearly seen that the fitting curves are good consistent with the experimental MC curves within $|B| < 50$ mT, and the intensity factors of each spin-pair interaction are displayed in Table S1. As the injection currents are reduced from 200 to 50 μA, the intensity factors a_1 and a_2 that represent the probabilities of ISC and RISC occurrences are positive and negative, respectively, leading to the unchanged sum of a_1 and a_2 values. This means that the MC curves within $|B| < 50$ mT are caused by the comprehensive effects of ISC from CBP polaron pairs and RISC from 4CzTPN-Ph CT excitons and the *B*-induced RISC process from ^{3}CT to ^{1}CT is dominant due to $|a_2| > a_1$. Additionally, since a_4 is greatly larger than $|a_3|$, TQA dissociation process is extremely weakened as compared to TQA scattering process, producing the vanished platform structure through utilizing the high electron mobility material of Bphen. The fitted results are consistent with above theoretical analysis, which further demonstrated that the spin-pair interactions occurring within

QW-TADF-OLEDs can be truly mediated by the electron mobility.

Table S1

Summary of parameters to fit the data curves in Fig. S4e

Current	a_1	a_2	a_3	a_4
200 μA	0.08631	-0.10976	-0.41751	2.11422
150 μA	0.09096	-0.23769	-0.44983	2.76546
100 μA	0.10082	-0.33249	-0.49649	3.29108
50 μA	0.11049	-0.42204	-0.53261	3.56868

Table S2

Summary of parameters for QW-TADF-OLEDs with *N* = 3, 5, 7, and 9.

Number of QW	3	5	7	9
Number of PBL	4	6	8	10
Thickness of each PBL	7.5 nm	5 nm	3.75 nm	3 nm
Number of emission	3	3	1	1
Emitting layer	CBP *m*-MTDATA/CBP 4CzTPN-Ph	CBP *m*-MTDATA/CBP 4CzTPN-Ph	4CzTPN-Ph	4CzTPN-Ph
EL peak	390 nm 490 nm 590 nm	390 nm 490 nm 590 nm	590 nm	590 nm

Notes and references

1 H. Oevering, J. W. Verhoeven, M. N. Paddon-Row, E. Cotsaris, N. S. Hush, *Chem. Phys. Lett*., 1988, **143**, 488-495.

2 Z. Y. Lu, Y. Hou, J. Xiao, H. S. Xu, *Displays*, 2014, **35**, 247-251.

3 S. M. Liu, B. Li, L. M. Zhang, H. Song, H. Jiang, *Appl. Phys. Lett*., 2010, **97**, 083304.

4 E. Y. Choi, J. H. Seo, H. M. Kim, K. H. Lee, H. J. Kang, S. S. Yoon, Y. K. Kim, *Jpn. J. Appl.*

122 *Phys*., 2011, **50**, 01BC07.

123 5 Y. Q. Li, M. K. Fung, Z. Y. Xie, S. T. Lee, L. S. Hung, J. M. Shi, *Adv. Mater*., 2002, **14**,

124 1317-1321.

125 6 N. N. Wang, J. S. Yu, Y. Zang, J. Huang, Y. D. Jiang, *Sol. Energy Mater. Sol. Energy*

126 *Mater. Sol. Cells*, 2010, **94**, 263-266.

127 7 Y. B. Chen, W. Y. Jia, J. Xiang, D. Yuan, Q. S. Chen, L. X. Chen, Z. H. Xiong, *Org.*

128 *Electron*., 2016, **39**, 207-213.